Proc. R. Soc. Lond. A **429**, 459–479 (1990)
Printed in Great Britain

High strain-rate shear response of polycarbonate and polymethyl methacrylate

BY N. A. FLECK, W. J. STRONGE AND J. H. LIU

University Engineering Department, Trumpington Street, Cambridge CB2 1PZ, U.K.

(*Communicated by I. M. Ward, F.R.S. – Received 2 August* 1989)

[Plates 1 and 2]

The high strain rate response of polycarbonate (PC) and polymethyl methacrylate (PMMA) are measured using a split Hopkinson torsion bar for shear strain rates $\dot{\gamma}$ from 500 s^{-1} to 2200 s^{-1}, and temperatures in the range -100 °C to 200 °C. The yield and fracture behaviours are compared with previous data and existing theories for $\dot{\gamma} < 1\ s^{-1}$. We find that PC yields in accordance with the Eyring theory of viscous flow, for temperatures between the beta transition temperature $T_\beta \approx -100$ °C and the glass transition temperature $T_g = 147$ °C. At lower temperatures, $T < T_\beta$, backbone chain motion becomes frozen and the shear yield stress is greater than the Eyring prediction. Strain softening is an essential feature of yield of PC at all strain rates employed. Polymethyl methacrylate fractures before yield in the high strain rate tests for $T < 80$ °C, which is close to the glass transition temperature $T_g = 120$ °C. It is found that the fracture stress for both materials obeys a thermal activation rate theory of Eyring type. Fracture is thought to be nucleation controlled, and is due to the initiation and break down of a craze at the fracture stress τ_f. Examination of the fracture surfaces reveals that failure is by the nucleation and propagation of inclined mode I microcracks which link to form a stepped fracture surface. This reveals that failure is by tensile cracking and not by a thermal instability in the material. The process of shear localization is fundamentally different from that shown by steel and titanium alloys.

1. INTRODUCTION

Polycarbonate (PC) and polymethyl methacrylate (PMMA) are transparent amorphous polymers which are commonly used for protective equipment such as eye goggles, windshields and body armour. PC has a greater resistance to ballistic perforation than PMMA. Indeed, its ballistic resistance is greater than that of aluminium according to Radin & Goldsmith (1988). In the present paper it is shown that the main reason for the impressive ballistic performance of PC is its high ductility at high strain-rates. Premature failure of PC (or PMMA) does not occur by thermally induced shear localization. This contrasts with some metals, where adiabatic shear leads to premature fracture at high strain rates.

A few studies have been made of the compressive yielding behaviour of polymers at high strain rates using a Hopkinson pressure bar, for example Kolsky (1949), Billington & Brissenden (1971), and Steer (1985). The technique is beset

by the problem of friction between the specimen and anvils. This results in a non-uniform stress state in the specimen. Progress to overcome the problem has been made by Briscoe & Nosker (1984) and Walley *et al.* (1989) by the successful use of lubricants. Torsion tests on short tubes do not suffer from this problem; the top and bottom faces of the specimen are glued to rigid anvils, the stress state is relatively uniform, and large shear strains can be imposed depending upon the ratio of specimen diameter to height.

The outline of the paper is as follows. First, we review current knowledge on the yielding and fracture of PC and of PMMA. The test method for high strain rate tests is outlined, and the shear stress–strain response of PC is described. We evaluate the ability of existing yield theories to account for the influence of temperature T and strain rate $\dot{\gamma}$ upon the yield stress of PC. The stress–strain response of PMMA is then reported, and the fracture behaviour of PC and PMMA is described. Finally, fractographic evidence and a shear localization calculation show that fracture of these polymers is by tensile microcracking and not by a thermal instability.

1.1. *Yielding of PC and PMMA*

Amorphous polymers such as PC and PMMA yield by a thermally activated process (see for example, Kinloch & Young 1983; Ward 1983). At a temperature of absolute zero thermal activation is absent; then, PC and PMMA exhibit the ideal strength $\tau/G \approx \frac{1}{7}$, where values for the shear stress τ and shear modulus G are extrapolated to absolute zero.

Recent work by Donald and co-workers (Donald & Kramer 1982; Donald *et al.* 1982) has shown that the tendency for an amorphous polymer to undergo crazing or shear yielding is governed largely by the polymer chain free length between entanglements, l. The chain free length gives a measure of the maximum extension of the polymer network without chain slippage or scission. When l is less than approximately 20 nm shear yielding occurs rather than crazing. At longer lengths, crazing occurs. For PC, l equals approximately 11 nm while for PMMA l equals approximately 19 nm (Donald & Kramer 1982). Both PC and PMMA undergo shear yielding or crazing depending upon temperature, strain rate and stress state. For example, both PC and PMMA undergo crazing from a sharp notch under impact loading, as reviewed by Kinloch & Young (1983). Under uniaxial tension at a strain rate of approximately $10^{-3}\,\mathrm{s}^{-1}$, crazing gives way to yielding at a ductile–brittle transition temperature of approximately $-200\,^{\circ}\mathrm{C}$ for PC and approximately 45 °C for PMMA.

1.2. *Yield of PC*

Consider first the yield behaviour of PC. The following physical picture of the yield process has emerged, notably from the work of Bauwens (1972), Argon (1973), Ward (1983), and G'Sell (1985). At temperatures below the beta transition temperature $T_\beta \approx -100\,^{\circ}\mathrm{C}$ (dependent upon strain rate), chain motion of PC is restricted to mainly rotation of the methane side groups. At temperatures above T_β, benzene groups in the main chain can also rotate; backbone chain motion is constrained to occur in an elastic tube defined by the other molecules. When the

temperature is increased to the glass transition temperature $T_g \approx 150$ °C, the van der Waals bonds between the backbone chains melt. At higher temperatures the material behaves as a rubber, with structural memory due to entanglement points.

The Ree–Eyring (1958) theory of viscous flow has been used with considerable success at correlating the yield and creep response of PC. The theory predicts that the strain rate $\dot{\gamma}$ due to an applied shear stress τ is given by:

$$\dot{\gamma}/\dot{\gamma}_0 = 2\exp(-Q/kT)\sinh(\tau v/kT), \tag{1}$$

where Q is a thermal activation energy, v is the so-called activation volume and $\dot{\gamma}_0$ is a constant. Usually $\tau v/kT \gg 1$ and equation (1) reduces to:

$$\dot{\gamma}/\dot{\gamma}_0 = \exp[-(Q-\tau v)/kT]. \tag{2}$$

It has been difficult to relate measured values of Q and v to microstructural parameters. Bauwens-Crowet *et al.* (1972) have shown a correlation between the activation energy for shear yielding of PC and the activation energy for molecular relaxations. They performed compression and tensile tests, and used a strain rate $\dot{\epsilon}$ in the range $10^{-4}\ \mathrm{s}^{-1} < \dot{\epsilon} < 1\ \mathrm{s}^{-1}$, and a temperature T, $-140\ °\mathrm{C} < T < 120\ °\mathrm{C}$. A two-part Eyring model correlated the data successfully: they used a lumped parameter model and modelled the response by two Eyring elements in parallel. They found that one element (termed α) dominated for $-50\ °\mathrm{C} < T < T_g$. The thermal activation energy Q_α for this process did not correlate with the activation energy for the glass transition relaxation in dynamic damping experiments. This suggests that the yielding process at large strains is fundamentally different from the anelastic behaviour at low strains. At $T < -50$ °C, the second Eyring element (termed β) is significant, with $Q_\beta = 40.1\ \mathrm{kJ\ mol^{-1}}$; this is comparable with the activation energy of $33.4\ \mathrm{kJ\ mol^{-1}}$ for the beta relaxation from dielectric measurements, Locati & Tobolsky (1970). Bauwens-Crowet *et al.* argued that the same molecular mechanism governed the low-temperature yield behaviour and the beta relaxation. A modification of the theory taking into account a distribution of beta relaxation times improved the quantitative link between the β yield process and the dynamic mechanical beta relaxation.

The measured value for the shear activated volumes v for both the α and β Eyring yield processes is of the order 3–6 nm^3 (Ward 1983; Bauwens-Crowet *et al.* 1972; Haward and Thackray 1968). This is much larger than the volume of a monomer unit, and suggests that yielding involves the cooperative movement of a large number of chain segments. Robertson (1966), Argon (1973) and Brown (1971) have each suggested microstructural yielding models based upon various kinematically admissible deformation modes. For example, Argon considers plastic deformation to occur by the kinking of molecular chains. The activation energy Q is the energy required to form two wedge disclination loops at both corners of the kink. Thus Q is of the form,

$$Q = C\omega E v, \tag{3}$$

where E is Youngs modulus, $\omega \approx 1$ is the angle of the wedge disclination, v is the shear activation volume, and C is a numerical constant of order unity.

Argon's model can be considered to be a special case of the Eyring theory where

Q depends upon the elastic modulus. The essential idea which appears to be correct from a growing amount of experimental evidence (see G'Sell (1985) for a review) is that polymer plasticity is controlled by the thermally activated cooperative motion of several chain segments against the elastic constraint of the surrounding matrix. For a moderate range of test temperatures below T_g, the elastic modulus is almost constant. Thus Q is approximately constant by equation (3) and the approaches of Argon and Eyring cannot be clearly distinguished at a curve-fitting level. A detailed comparison of the Argon and Eyring approaches has been given by Ward (1983).

1.3. *Yielding of PMMA*

The tensile and compressive yield stresses of PMMA vary with temperatures T and with strain rate $\dot{\epsilon}$, in a similar manner to that described above for PC. Bauwens-Crowet (1973) has successfully described yield using a two element Eyring equation. The thermal activation energy Q_β for the beta process is found to be comparable with that from mechanical damping measurements (Bauwens-Crowet 1973; Iwayanagy & Hideshima 1953; Thompson 1968). We conclude that the same microstructural mechanism operates in the two cases. The tensile yield data for PMMA does not cover as wide a range of experimental conditions as for PC, as PMMA undergoes brittle fracture before yielding at $T \leqslant 50$ °C, $\dot{\epsilon} \leqslant 1\ \mathrm{s}^{-1}$.

The beta relaxation process for PMMA is associated with the temperature at which motion of the main backbone chain becomes possible, in addition to motion of the side ester groups. The transition temperature T_β is in the range of $0\ °\mathrm{C} \leqslant T_\beta < 30\ °\mathrm{C}$ and is a more minor relaxation than for PC (Sherby & Dorn 1958).

Correlation of the yield behaviour with the dynamic relaxation response is more successful for PMMA and PC than for other polymers. The subject has been reviewed comprehensively by Kinloch & Young (1983) and by Ward (1983).

1.4. *Fracture of PC and PMMA*

Unnotched tensile specimens of PC and PMMA fail by the nucleation and growth of crazes. A crack forms by breakdown of a craze and failure is by propagation of one or more cracks; the cracks advance by crazing at the tip. This failure sequence is described in more detail by Hull (1975) and by Kinloch & Young (1983). When craze nucleation and catastrophic growth occur at a stress below the yield stress the polymer behaves in an elastic–brittle manner. Alternatively, failure may occur after general yield in which case the polymer behaves in a ductile manner.

Zhurkov (1965) was the first to show that the fracture strength of PMMA may be described by an equation similar to the Ree–Eyring (1958) theory. The shear strength τ_f is assumed to be related to shear strain rate $\dot{\gamma}$ and temperature T by an equation analogous to (2),

$$\dot{\gamma}/\dot{\gamma}_0 = \exp\left[-(Q_f - \tau_f v_f)/kT\right], \tag{4}$$

where $\dot{\gamma}_0$ is a constant and v_f is the shear activation volume for fracture. He demonstrated that the activation energy Q_f correlates reasonably well with the activation energy for thermal degradation of PMMA.

A more detailed model of fracture by the thermally activated nucleation and growth of crazes has been given by Argon & Hannoosh (1977). The model requires several microstructural parameters for its application, and is based upon an approximate early model of void growth in plastic bodies by McClintock & Stowers (1970).

Equation (4) is a useful description when fracture is controlled by the nucleation of crazes; a fracture mechanics approach is more appropriate when crack propagation is the critical step.

2. Split Hopkinson torsion bar tests

A split Hopkinson torsion bar was used to determine the shear stress τ against shear strain γ response of PC and PMMA, at strain rates in the range 500 s^{-1} to 2200 s^{-1}, and temperatures in the range -100 °C to 200 °C. The torsion bar was designed to apply a 'square' pulse of shear strain-rate for a period of *ca.* 1 ms to a tubular specimen of waisted section, figure 1, and to record the variation in shear stress developed in the specimen. Full details about the test rig are given by Clyens *et al.* (1982). Brief notes about the test method including the environmental chamber are reported in Appendix A. The shear stress τ is defined on the basis of the original cross section of the tubular specimen, as described in Appendix A. Shear strain γ is given by $\gamma = \tan\phi$ where ϕ is the angle of simple shear.

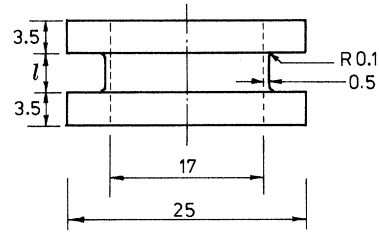

Figure 1. Torsion specimen with dimensions in millimetres. Gauge length l depends on the required strain rate; i.e. $l = 4$ mm for $\dot{\gamma} < 800$ s^{-1} and $l = 1.5$ mm for $\dot{\gamma} > 800$ s^{-1}.

3. Test materials

Specimens were machined from 25 mm diameter extruded bars of PC and PMMA. The PC material is bisphenol A polycarbonate. It has a weight average molecular mass $M_w = 21\,600$ and $M_n = 9420$, and originated as Bayer Makrolon granules. The PMMA material has a molecular mass $M_w = 1.44 \times 10^6$ and $M_n = 2.47 \times 10^5$. The molecular masses were measured by gel permeation chromatography, using tetrahydrofuran as solvent, and Mark–Houwinck parameters for the calibration.

Differential scanning calorimetry was used to measure the glass transition temperature T_g for both materials. We found $T_g = 147$ °C for PC and $T_g = 120$ °C for PMMA, using a heating rate of 10 °C min^{-1}. Both polymers are linear chain amorphous thermoplastics. They were tested in the as-received state.

4. Deformation behaviour of PC

The influence of temperature on the τ–γ response of PC is given in figure 2 for $\dot{\gamma} \approx 550\ \mathrm{s}^{-1}$ and $\dot{\gamma} \approx 2000\ \mathrm{s}^{-1}$. In this and in subsequent figures a cross at the end of the τ–γ curve designates specimen fracture. In all tests yield occurred before specimen fracture. The influence of strain-rate on the deformation response at $T = 20\ ^\circ\mathrm{C}$ is shown in figure 3; these results include a slow strain-rate $\dot{\gamma} = 1 \times 10^{-3}\ \mathrm{s}^{-1}$. The slow strain-rate test was performed using a screw driven torsion machine.

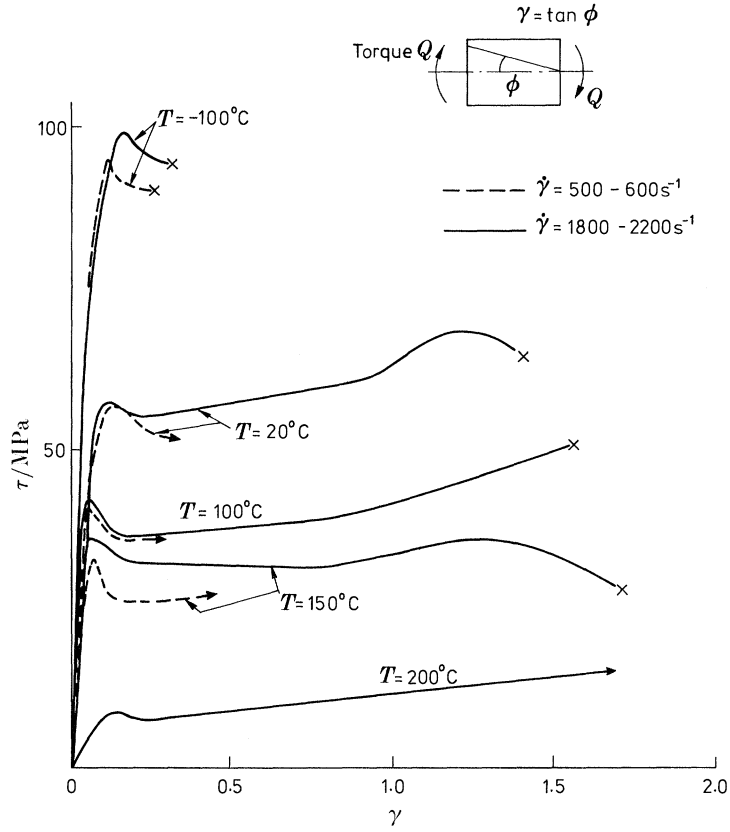

Figure 2. Effect of temperature and strain rate on stress–strain response of PC. Crosses denote fracture.

Strain rate has only a modest influence on the upper yield stress τ_y as shown in figures 2 and 3. For example, at $T = 20\ ^\circ\mathrm{C}$, τ_y increases by 43% when $\dot{\gamma}$ is increased by more than six orders of magnitude from $1 \times 10^{-3}\ \mathrm{s}^{-1}$ to $1830\ \mathrm{s}^{-1}$.

At $\dot{\gamma} \approx 2000\ \mathrm{s}^{-1}$ the maximum imposed strain was sufficient to cause specimen fracture at all temperatures less than 200 °C. Fracture did not occur at $\dot{\gamma} \approx 550\ \mathrm{s}^{-1}$ because the apparatus restricted the allowable range of nominal strain in these specimens. The observed deformation response in these tests can be related to the micromechanisms of polymer flow in the following manner.

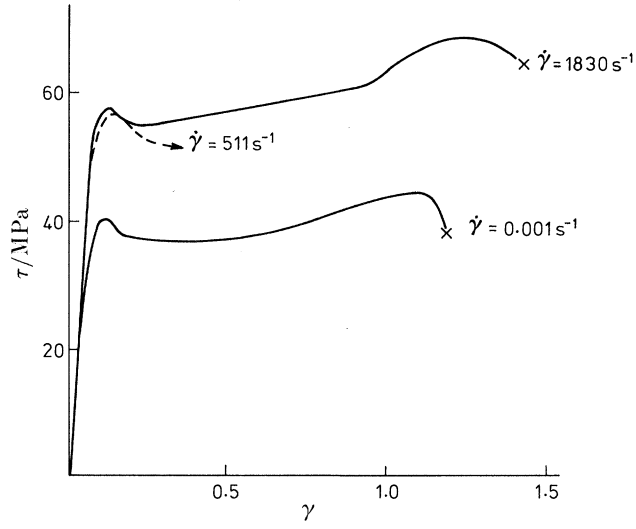

FIGURE 3. Effect of strain-rate on stress–strain response of PC at $T = 20$ °C.

At temperatures above the glass transition temperature $T_g = 147$ °C, van der Waals bonds between the PC molecules have melted and the material is rubbery. At temperatures below the glass transition temperature T_g, thermally activated plastic deformation of polymers involves relative sliding of the main backbone molecules, as described in the introduction. For temperatures in the range -50 °C to 150 °C deformation typically consists of four distinct stages. These stages were observed directly at $T = 20$ °C and $\dot{\gamma} = 1 \times 10^{-3}$ s^{-1} by a sequence of photographs of a specimen marked by axial lines, shown schematically in figure 4.

1. An initial homogeneous elastic response at small strains. An upper yield stress τ_y at $\gamma = 0.1$–0.2 terminates this stage.

2. The macroscopic shear stress drops by roughly 8% to an almost constant value τ_p. This strain-softening is associated with the formation of a shear band. Material in a thin shear band deforms until it attains a shear strain of $\gamma = 0.7$–1.0. Thereafter the shear strain in the band is constant but the band broadens along the axis of the specimen as the nominal shear strain increases; this occurs at an almost constant propagation stress τ_p. Additional shear bands may nucleate, and grow at the expense of the existing band.

3. When the shear band or bands have consumed the gauge length of the specimen, the test piece again strain-hardens homogeneously.

4. Finally, the specimen fractures at a fracture stress τ_f, and fracture strain $\gamma_f = 1.5$–2.0.

These four stages of deformation are also present in the high strain-rate tests, at test temperatures T in the range -50 °C to 150 °C. The first two stages are shown by schematic diagrams transcribed from high-speed photographs of a test at $T = 20$ °C, $\dot{\gamma} = 1050$ s^{-1}, see figure 5. These photographs were taken *in situ* using an IMACON high-speed camera, triggered from the strain gauge of the output torsion bar. The photographs show the initial uniform deformation (stage

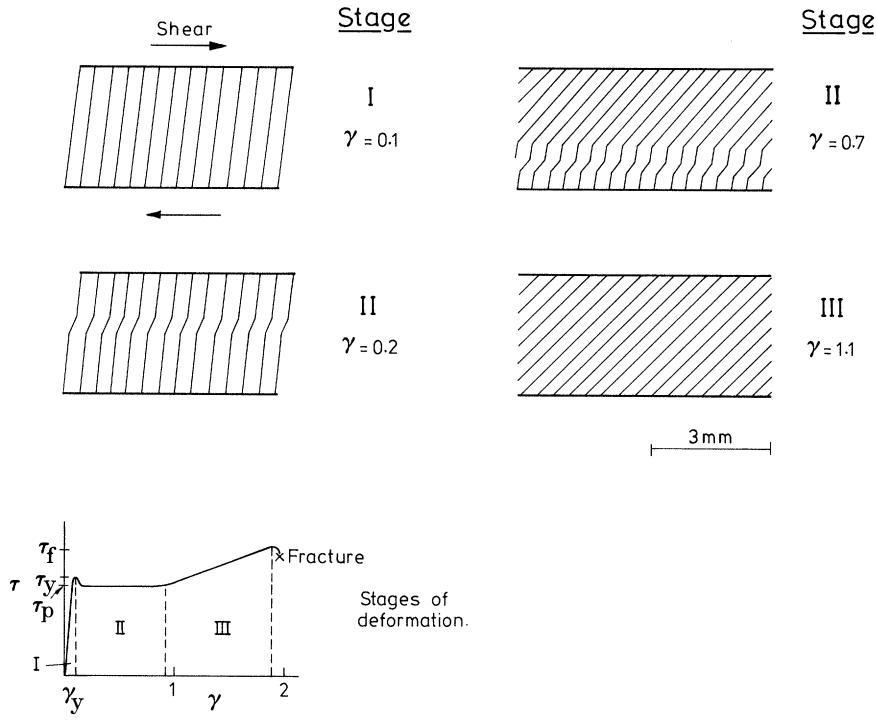

FIGURE 4. Non-homogeneous shear deformation of PC at $\dot{\gamma} = 10^{-3}\,\mathrm{s}^{-1}$ and $T = 20\,^{\circ}\mathrm{C}$. The diagrams are drawn directly from photographs, and show the deformation of axial marker lines.

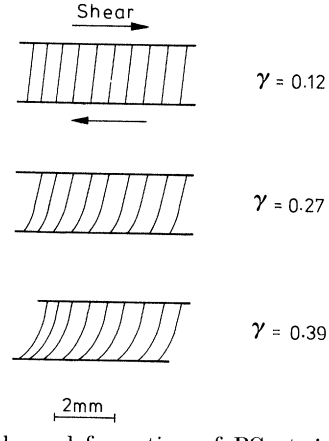

FIGURE 5. Non-homogeneous shear deformation of PC at $\dot{\gamma} = 1050\,\mathrm{s}^{-1}$ and $T = 20\,^{\circ}\mathrm{C}$; the curved marker bands are reproduced from high-speed photographs. Gauge length of specimen $l = 2$ mm.

I) for $\gamma < 0.2$, giving way to shear banding (stage II) at higher strains. With increasing nominal γ the shear band propagates along the axis of the specimen. Material outside of the yielded region remains elastic.

G'Sell & Gopez (1985) have also observed the four stages of shear deformation of PC at low strain rates $\dot{\gamma} = 3 \times 10^{-5}\,\mathrm{s}^{-1}$ to $3 \times 10^{-2}\,\mathrm{s}^{-1}$, and temperatures in the

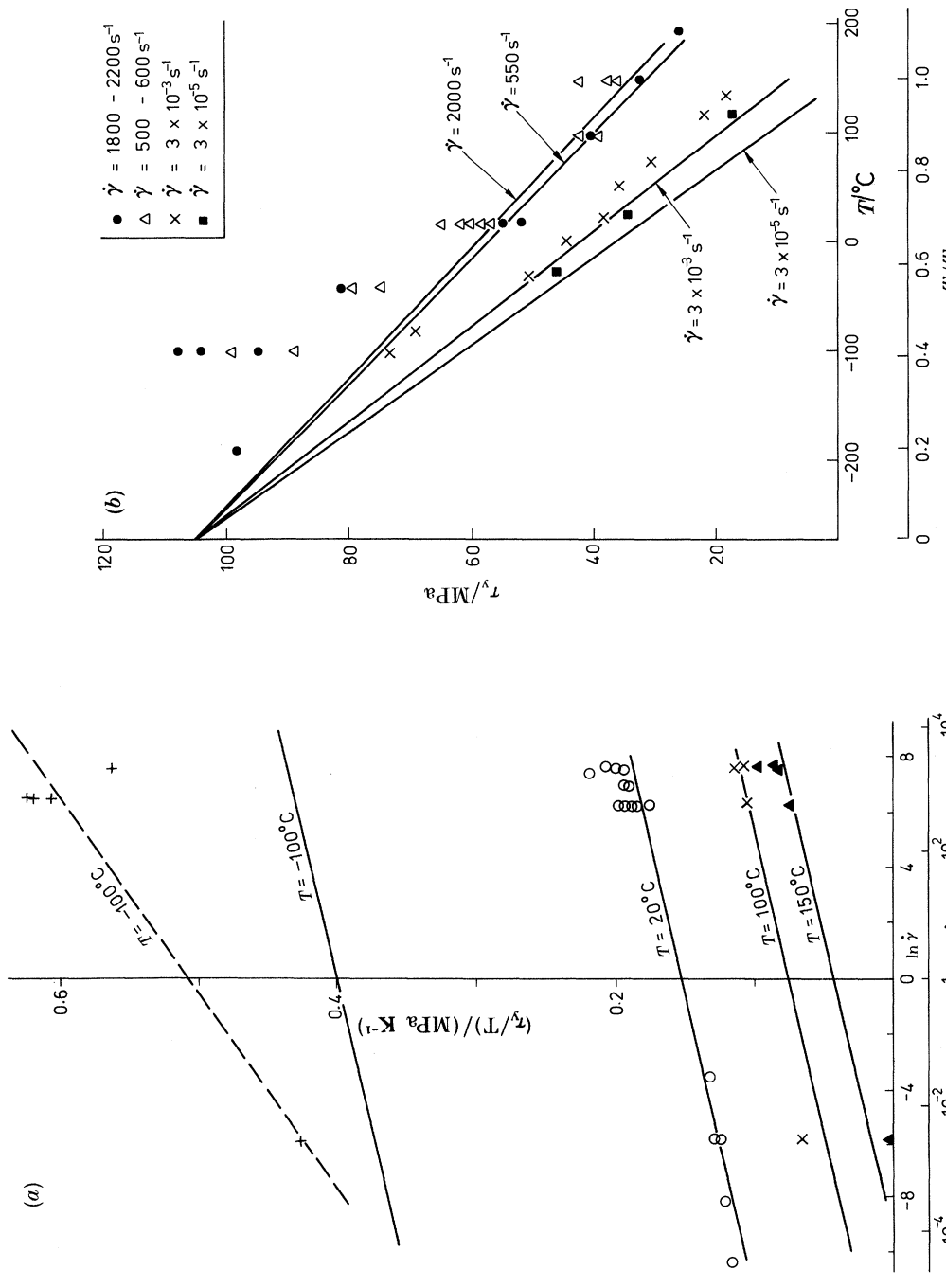

FIGURE 6. (*a*) Effect of strain-rate on upper yield stress τ_y of PC. The solid lines are an Eyring fit; the dotted line is a best fit to the experimental data. Data for $\dot{\gamma} < 1\ \mathrm{s^{-1}}$ are taken from G'Sell & Gopez (1985). (*b*) Effect of temperature on upper yield stress τ_y of PC. The solid lines are an Eyring fit. Data for $\dot{\gamma} = 3 \times 10^{-3}\ \mathrm{s^{-1}}$ and $3 \times 10^{-5}\ \mathrm{s^{-1}}$ are taken from G'Sell & Gopez (1985).

range -100 °C to 150 °C. They tested plate specimens in simple shear. It is thought that torsion tests on tubular specimens give more reliable shear data, since the stress state is more uniform in tubular specimens than in plate specimens.

4.1. *Yield response of polycarbonate*

The high strain rate yield response of PC fits a single stage Eyring equation tolerably well for temperatures in the range -20 °C $< T <$ 150 °C and $10^{-3} < \dot{\gamma} <$ 2000 s^{-1} as shown in figure 6*a* and *b*. The figures contain a best fit to equation (2) with $Q = 191$ kJ mol^{-1}, $v = 3.0$ nm^3. At lower temperatures τ_y is larger than predicted, see figure 6*b*, and a two stage Eyring fit is required as suggested by Bauwens-Crowet *et al.* (1972). Bauwens-Crowet *et al.* argue that as the temperature is reduced through the beta transition, main motion becomes frozen, leaving only movement of the methyl side groups. The experimental data of the present study shows too much scatter to warrant a detailed attempt to fit a two-stage Eyring model, but the data show the same qualitative features as that described for PC at low compressive strain rates by Bauwens-Crowet *et al.* (1972). At $T = -100$ °C, the slope of the τ_y/T against $\ln \dot{\gamma}$ graph in figure 6*a* is steeper than at $T \geqslant 20$ °C. The Eyring equation (3) gives a slope equal to k/v; thus the data of figure 6*a* suggests a decreased volume activation energy $v = 2.0$ nm^3 at $T = -100$ °C compared with $v = 3.0$ nm^3 at $T \geqslant 20$ °C. This implies a more localized deformation micromechanism at the lower temperature. The measured value for $Q = 234$ for kJ mol^{-1} at $T \geqslant 20$ °C is in fair agreement with the measured value $Q_\alpha = 316$ kJ mol^{-1}, by Bauwens-Crowet *et al.* (1972).

We observe little variation in shear modulus G with temperature and strain rate for -100 °C $< T <$ 150 °C and 500 $s^{-1} < \dot{\epsilon} <$ 2200 s^{-1}. The Hopkinson bar method is not well suited to the determination of G, as discussed by Clyens *et al.* (1982). Thus, given the scatter in measurements of τ_y and of G, we are unable to state whether the thermal activation energy Q varies linearly with G, as suggested by equation (3).

The source of the scatter in the high strain rate torsion tests comes from a number of sources, including (i) variations in material response due to different amounts of machining damage during manufacture, and (ii) slight variations in test temperature in the specimen. In the high-temperature tests where $T \geqslant 150$ °C, the specimens suffer a small amount of creep during set-up of the test: these tests are particularly difficult to perform and the results should be treated with caution.

5. Deformation response of PMMA

The effect of temperature upon the τ–γ response of PMMA at high strain rate is shown in figure 7. The influence of strain rate upon the behaviour at $T = 20$ °C is given in figure 8.

Consider first the high strain rate response, $500 < \dot{\gamma} < 2200$ s^{-1}, figure 7. At $\dot{\gamma} \approx 550$ s^{-1}, PMMA fractures before an upper yield point is reached for $T < 80$ °C; at temperatures in the range 80 °C $\leqslant T \leqslant T_g = 120$ °C, it displays an upper yield stress and large failure strains $\gamma_f > 0.5$. At higher temperatures it behaves in a rubbery fashion. At $\dot{\gamma} \approx 2000$ s^{-1}, PMMA fractures before yield

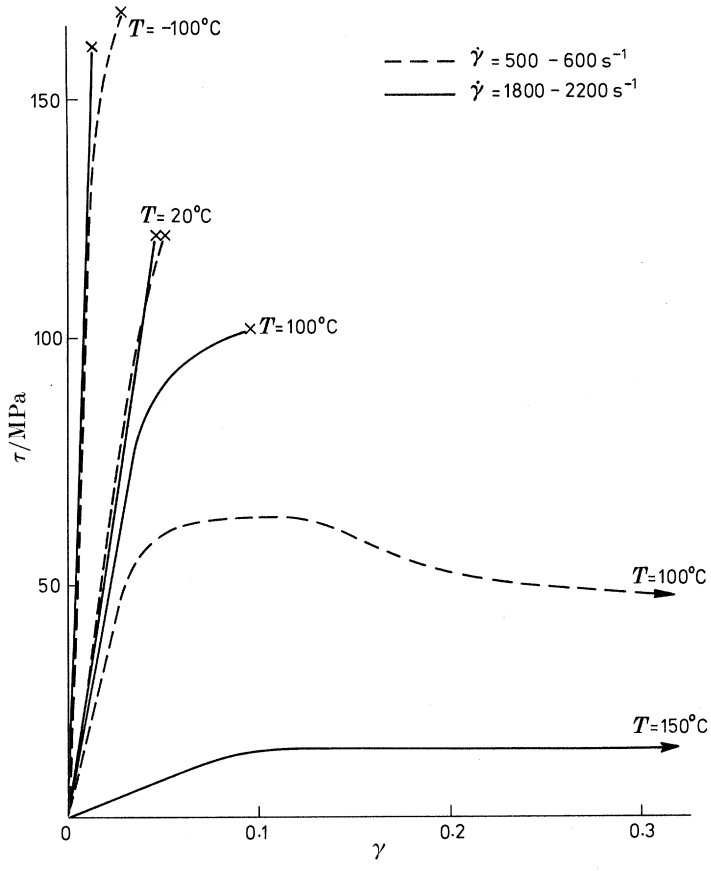

FIGURE 7. Effect of temperature and strain-rate on stress–strain response of PMMA. Crosses denote fracture.

at all test temperatures $T \leqslant 100$ °C. At $T = 150$ °C, the temperature is above T_g and it behaves as a rubber.

Now consider the influence of strain rate upon the response at $T = 20$ °C, figure 8. At quasi-static strain rates, $\dot{\gamma} = 10^{-3}$ s^{-1}, fracture occurs much later than yielding: the ductility is high with $\gamma_f > 1$. At high strain rates, $\dot{\gamma} \geqslant 500$ s^{-1}, brittle fracture occurs before yielding. There is a delicate balance between shear yielding and craze-induced fracture in PMMA. At low temperatures and high strain rates crazing is favoured, while shear yielding precedes crazing at high temperatures and at low strain rates. This is in agreement with previous studies on PMMA (see Kinloch & Young (1983) for a review).

In most of the tests on PMMA in the present study, fracture precedes yielding. There is insufficient data to determine the ability of the Eyring theory in describing the yield response of PMMA. This issue has already been examined by Bauwens-Crowet (1973), and has been discussed in the introduction. Sufficient data have been obtained in the present study to examine the influence of temperature and strain rate upon the fracture response of PMMA and PC.

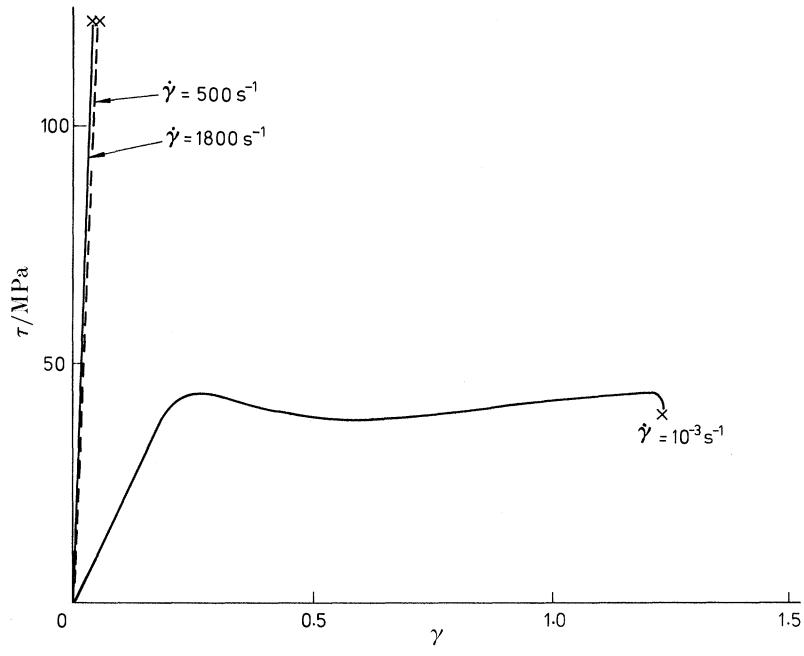

FIGURE 8. Effect of strain-rate on stress–strain response of PMMA at $T = 20$ °C.

6. Fracture response of PC and PMMA

Fracture of PC and PMMA is by the nucleation and breakdown of crazes. Zhurkov (1965) has suggested that the fracture stress of polymers obeys a thermal activation law of the form given in equation (4). This equation predicts a linear relation between τ_f/T and $\ln \dot{\gamma}$ with slope k/v_f, where τ_f is the shear fracture stress and v_f is the shear activation volume for fracture. Data for the fracture stress of PMMA, plotted in figure 9, supports equation (4). The best fitting straight lines in figure 9 are defined by equation (4) with $v_f = 0.46$ nm^3, $Q_f = 54$ kJ mol^{-1}.

Equation (4) also predicts a linear relation between τ_f and T for a given $\dot{\gamma}$. The data support this for PMMA, for $T \leqslant T_g$, as shown in figure 10*a*. Bearing in mind the degree of scatter in the high strain rate tests, we conclude tentatively that an equation of Eyring form, equation (4), is able to describe the fracture stress of PMMA.

Bauwens-Crowet (1973) has observed a beta relaxation at $T \approx 20$ °C in the yield of PMMA, associated with side chain motions of the ester group. This relaxation appears to have little influence on the fracture behaviour of PMMA: a single-stage Eyring equation suffices. The shear activation volume $v_f = 0.46$ nm^3 for fracture of PMMA is an order of magnitude less than the values $v = 4$–6 nm^3 observed in the tensile and compressive yield of PMMA, by Haward & Thackray (1968) and by Bauwens-Crowet (1973). This suggests that much less cooperative motion of chain segments is required for nucleating crazing (and thereby causing fracture) than for nucleating yield.

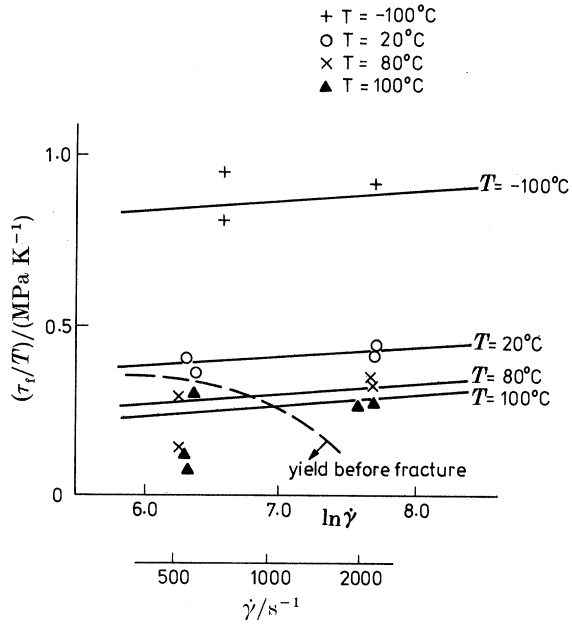

FIGURE 9. Effect of strain-rate on fracture stress τ_f of PMMA. The solid lines represent an Eyring fit to the fracture data.

A plot of fracture stress τ_f against T for PC is included in figure 10*a*. Again, an equation of Eyring form appears to fit the limited data for $T < T_g$: the full lines in figure 10*a* are given by equation (4) using the best-fitting values $v_f = 3.9$ nm^3 $Q_f = 276$ kJ mol^{-1}. These values are similar to the measured values for the yield of PC where $v = 3.0$ nm^3 and $Q = 191$ kJ mol^{-1}. Since failure did not occur in the tests at $\dot{\gamma} \approx 550$ s^{-1}, there is insufficient data to warrant a plot of τ_f/T against $\ln \dot{\gamma}$ for PC.

6.1. *Ductility of PC and PMMA*

The strain to failure γ_f of PC and PMMA is compared in figure 10*b*. There is a marked difference in the responses of the two materials. The ductility, γ_f, of PC is more than an order of magnitude greater than that of PMMA for $0.4 < T/T_g < 0.8$. Also, the fracture strength of PMMA is nearly double that of PC for $T < T_g$, see figure 10*a*. We explain these results as follows.

Consider first PMMA. In the tests at high strain rate and $T < T_g$ fracture occurs before or soon after shear yielding: the ductility γ_f is low. At $T = 20$ °C $\approx T_\beta$ the ductility is sensitive to strain rate; at $\dot{\gamma} = 1.0 \times 10^{-3}$ s^{-1}, $\gamma_f = 1.2$ while at $\dot{\gamma} \geqslant 500$ s^{-1}, $\gamma_f \approx 0.05$. Unfortunately, no low strain rate data are available for PMMA at other temperatures. Polycarbonate shows a similar sensitivity to strain rate for temperatures near the beta transition, $T_\beta = -120$ °C, $(T_\beta/T_g = 0.4)$, see figure 10*b*. The strain to failure increases dramatically from 0.2 to greater than 1.5 as the temperature is increased through the beta transition.

The rapid switch in γ_f with $\dot{\gamma}$ and with T for PC at $T \approx T_\beta$ $(T_\beta/T_g = 0.4)$ is

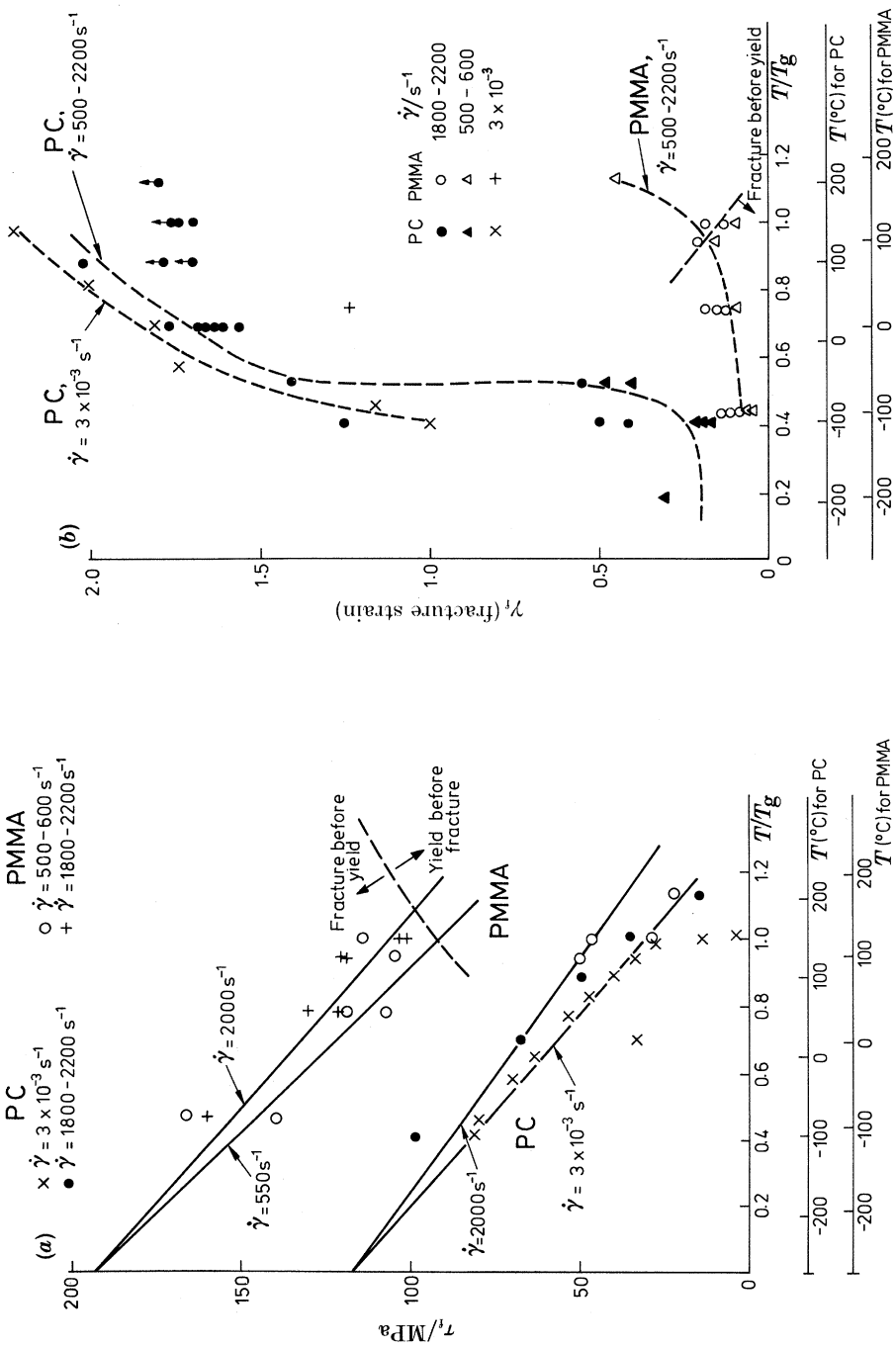

FIGURE 10. (*a*) Fracture stress of PC and PMMA throughout the temperature range. The solid lines represent Eyring fits. Data for PC at $\dot{\gamma} = 3 \times 10^{-3}$ s^{-1} are taken from G'Sell & Gopez (1985). (*b*) Fracture strain of PC and PMMA throughout the temperature range. Data for PC at $\dot{\gamma} = 3 \times 10^{-3}$ s^{-1} are taken from G'Sell & Gopez (1985).

associated with its strain softening response at yield. Failure occurs either before a shear band has established itself or after a shear band has propagated along the length of the specimen. Since the shear yield strain is approximately 0.1 while the shear strain in the shear band is of order unity, the failure strain is either less than 0.1 or exceeds unity.

PC possesses a high ductility at all strain rates investigated for $T \geqslant T_\beta \approx -120$ °C. It appears that the high impact resistance of PC is linked to the feature that it has an unusually low beta transition. By contrast, the beta transition of PMMA is near room temperature; under ambient temperatures it is ductile at low loading rates but brittle under impact conditions.

Details of the fracture mechanisms in PC and PMMA are now given, followed by a discussion of adiabatic heating in these materials.

6.2. *Fracture path*

Examination of the fracture surfaces using a scanning electron microscope (SEM) reveals that fracture of PC and PMMA is by the nucleation of crazes, followed by craze breakdown and microcrack growth. The microcracks grow by crazing at their tips and are oriented initially at 45° to the shearing direction, which is normal to the direction of maximum tensile stress. The microcracks coalesce to form a furrowed fracture surface. On the microscopic level the fracture surface is parallel to the plane of shear. Typical fracture surfaces are given in figures 11 and 12, plates 1 and 2, for PC and PMMA, respectively. Fracture surface development is shown schematically in figure 13.

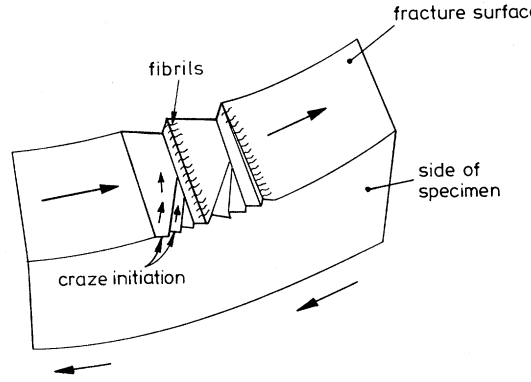

FIGURE 13. Schematic of fracture surface development in PC and PMMA. Crazes nucleate and breakdown into microcracks, initially orientated normal to the direction of maximum principal stress (i.e. at 45° to the shear direction).

It is unlikely that the microcracking occurs simultaneously around the periphery of the specimen: rather a macroscopic crack forms from several coalesced microcracks. The macrocrack unzips the remaining ligament by the same process of craze nucleation followed by craze breakdown and microcrack growth, at the tip of the macrocrack. Evidence for this is given in figure 11*d*, which shows an unfailed ligament of PC. For both PC and PMMA, the amount of

fibrillation at the tip of each microcrack increases with increasing temperature and strain rate, see figures 11 and 12. The increased crazing at high strain rate is consistent with the observations by Fuller *et al.* (1975) that high temperatures (of order 500 °C) are attained for a short time (about 100 μs) near the tip of a tensile crack growing at high velocity (200–600 m s^{-1}). The crack tip heating encourages fibrillation. Crazing was not discerned in the low strain rate ($\dot{\gamma} = 10^{-3}$ s^{-1}), room temperature tests on PC and on PMMA: the fibril length is too short to be resolved in a SEM, as discussed by Kinloch & Young (1983).

Brittle fracture due to the growth and coalescence of an array of tensile microcracks under remote shear has been analysed rigorously by Fleck (1990). The evolution of the cracks into curved profiles is calculated; crack coalescence is predicted for remote shear loading.

6.3. *Adiabatic heating*

Winter (1975) has suggested that shear fracture of PMMA is by a thermally induced shear instability. We argue that fracture of PC and PMMA is not by thermal instability but rather by the advance of tensile microcracks. First, we show that adiabatic heating does occur in the high strain-rate tests.

For adiabatic heating, the time taken for plastic deformation (i.e. the test time) is much less than the thermal diffusion time, t_d. The thermal diffusion time is defined as:

$$t_d \approx L^2/2\kappa,$$

where $\kappa \approx 1 \times 10^{-7}$ m^2 s^{-1} is the thermal diffusivity of PC and PMMA, and L is a characteristic dimension of the specimen from the centre of the deforming region to the nearest heat-sink. We assume that L is half the wall thickness of the torsion specimen $L \approx \frac{1}{2}t$. If the average strain imposed on the sample is unity then the condition for adiabatic heating is that the strain-rate exceeds the value

$$\dot{\gamma} > 2\kappa/L^2.$$

On substitution of typical values for κ and L we find, for both PC and PMMA, that adiabatic straining occurs for $\dot{\gamma} > 2$ s^{-1}. Hence the high strain-rate tests, $\dot{\gamma} > 10^2$ s^{-1}, are adiabatic, whereas the quasi-static tests $\dot{\gamma} \approx 10^{-3}$ s^{-1} are isothermal. Under adiabatic conditions the uniform temperature rise in the specimen ΔT is

$$\Delta T \rho c_v = \tau\gamma,$$

where the plastic work has been equated with an increase in internal energy. Here. ρ is the density and c_v is the specific heat capacity. For both PC and PMMA, ΔT is typically 30 °C per unit shear strain.

Now we address the issue whether failure of either polymer is by a thermal instability. Examination of the fracture surfaces given in figures 11 and 12 reveals that melting of the fracture surface has not occurred. Rather, failure is by brittle fracture. Further evidence against a thermal instability is provided by use of Bai's perturbation analysis of thermoplastic shear instability (Bai 1982). Bai shows that thermal softening leads to instability when it outweighs strain-hardening, such that the ratio B exceeds unity,

$$B = \tau|\partial\tau/\partial T|/(\rho c_v \partial\tau/\partial\gamma) > 1.$$

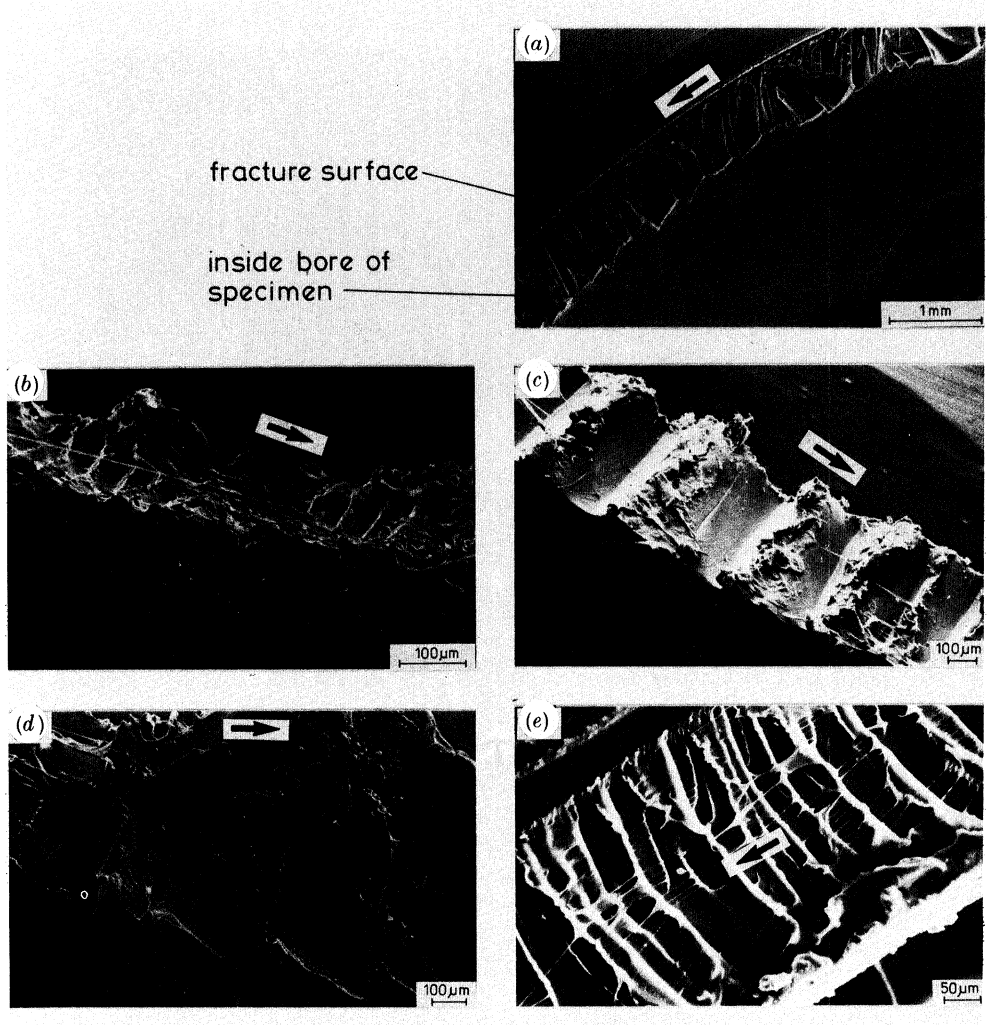

FIGURE 11. Fracture surfaces of PC. The arrow denotes the direction of motion of the top half of the specimen with respect to the displayed bottom half. (*a*) $T = 20$ °C, $\dot{\gamma} = 10^{-3}$ s^{-1}; (*b*) $T = -100$ °C, $\dot{\gamma} = 2100$ s^{-1}; (*c*) $T = 20$ °C, $\dot{\gamma} = 2100$ s^{-1}; (*d*) unfailed ligament of specimen, $T = 20$ °C, $\dot{\gamma} = 2100$ s^{-1}; (*e*) $T = 150$ °C, $\dot{\gamma} = 2100$ s^{-1}.

(*Facing p.* 474)

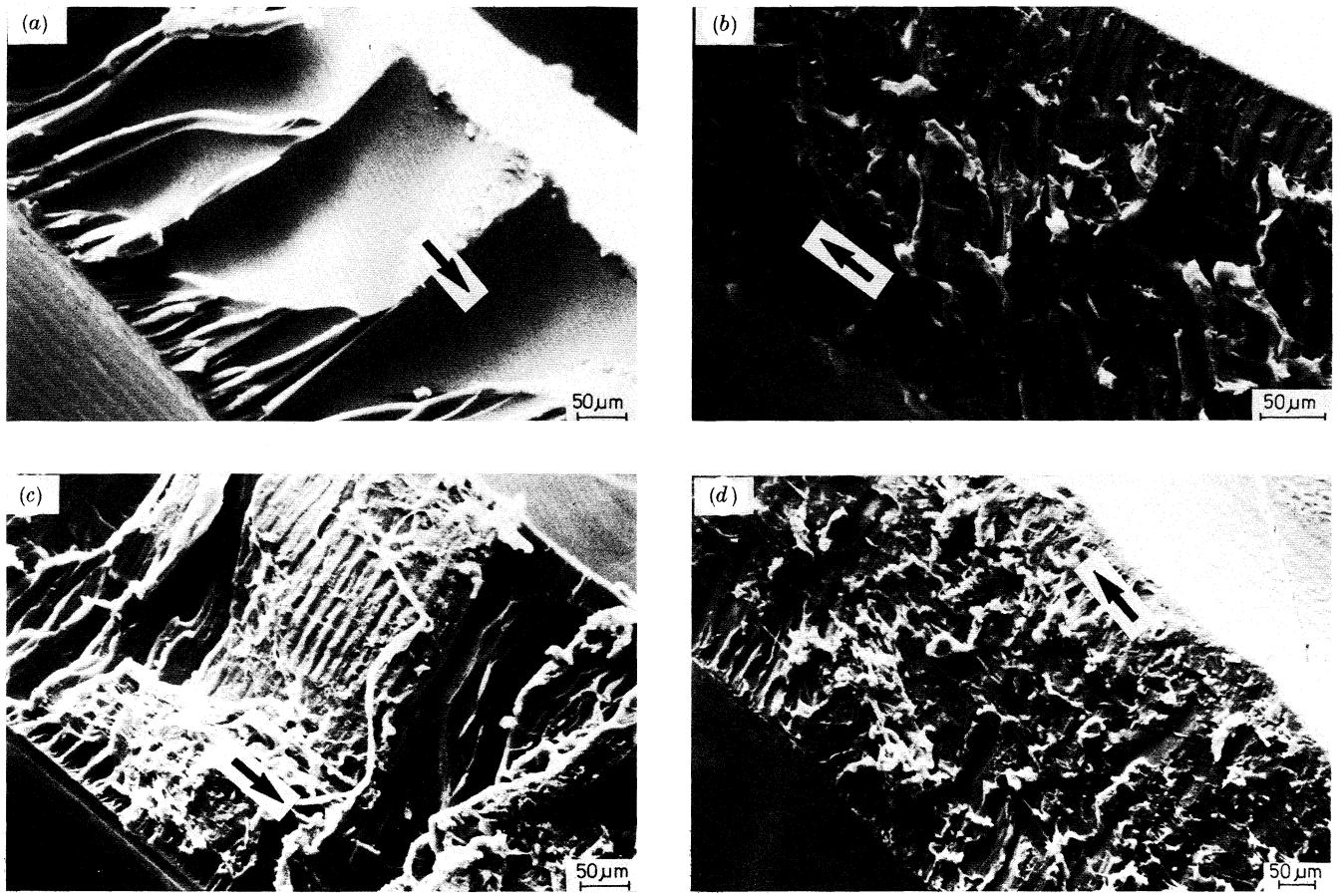

FIGURE 12. Fracture surface of PMMA. The arrow denotes the direction of motion of the top half of the specimen with respect to the displayed bottom half. (*a*) $T = 20$ °C, $\dot{\gamma} = 10^{-3}$ s^{-1}; (*b*) $T = -100$ °C, $\dot{\gamma} = 2100$ s^{-1}; (*c*) $T = 20$ °C, $\dot{\gamma} = 2100$ s^{-1}; (*d*) $T = 80$ °C, $\dot{\gamma} = 2100$ s^{-1}.

We calculate the ratio to be typically $B \approx 0.2$ for PC, assuming the following values $\tau = 50$ MPa, $|\partial\tau/\partial T| = 0.25$ MPa K^{-1}, $\rho c_v = 1.3 \times 10^6$ J m^{-3} K^{-1}, and $\partial\tau/\partial\gamma = 50$ MPa. The calculation is sensitive to the choice of strain-hardening rate $\partial\tau/\partial\gamma$ used. Here, we take the average rate for $T = 20$ °C and $\dot{\gamma} = 2000$ s^{-1}, and γ in the post strain-softening range 1.1 to 1.3, figure 2. We conclude that thermally induced instability does not occur in PC due to the stabilizing influence of orientation hardening. Similar arguments can be made for PMMA.

When thermoplastics such as PC and PMMA are subjected to uniaxial tension or compression several intersecting shear bands form on planes of maximum resolved shear stress. The shear bands block each other and lead to enhanced strain-hardening. Cottrell (1963) refers to the equivalent slip process in metals as 'turbulent flow'. The intersecting shear bands set up back stresses at intersection points leading to enhanced strain-hardening. This effect reduces further the likelihood of thermally induced localization of deformation.

7. Conclusions

High strain-rate torsion tests have been performed successfully on polycarbonate (PC) and polymethyl methacrylate (PMMA), using strain rates in the range $500\ \text{s}^{-1} < \dot{\gamma} < 2200\ \text{s}^{-1}$ and temperatures in the range $-100\ °\text{C} < T < 200\ °\text{C}$. The following conclusions have been drawn from these tests.

1. PC yields before fracture at all strain rates and temperatures examined. Yielding involves inhomogeneous deformation with the propagation of a softened shear band along the axis of the specimen; this is observed in both high strain rates $\dot{\gamma} \geqslant 500\ \text{s}^{-1}$ and at low strain rates, $\dot{\gamma} \approx 10^{-3}\ \text{s}^{-1}$. PMMA fractures before yield in the high strain rate tests for $T < 80$ °C.

2. For both PC and PMMA, the yield and fracture stresses at high strain rates can be described by an Eyring-type equation. In view of the scatter of the present results, further tests should be performed to confirm this conclusion.

Both PMMA and PC undergo a transition in fracture response near their beta transition temperatures. The yield stress rises and the ductility γ_f falls steeply when the test temperature is reduced through the beta relaxation temperature T_β. At temperatures near T_β, the fracture stress and ductility are sensitive to strain rate.

The difference in strain rate sensitivities of the fracture response shown by PMMA and PC at room temperature appears to be linked to the difference in their beta relaxation temperatures. The unusually low beta transition temperature of PC affords it large shear ductility over a wide range of temperatures and strain rates.

3. Fracture of PC and PMMA is by craze nucleation, followed by craze breakdown into tensile microcracks. The microcracks grow by craze formation at their tips and coalesce to form the fracture surface. Despite their low thermal diffusivities, fracture of these polymers is not due to a thermally induced shear instability since orientation hardening stabilizes the deformation.

We are grateful for fruitful discussions with Professors M. F. Ashby, A. S. Argon, M. C. Boyce and D. Tabor, and with Dr A. H. Windle. We thank Mr S. C. Wright for help with data reduction, and RAPRA Materials characterization service for performing the molecular mass measurements.

Appendix A. Test method

Tests were performed using a split Hopkinson torsion bar (figure 14). The 25 mm diameter titanium bar is 4.2 m long and is mounted vertically such that it can twist freely. The bar is split at 1.67 m from the lower end and the test specimen is glued between the two parts, using cyano-acrylate adhesive.

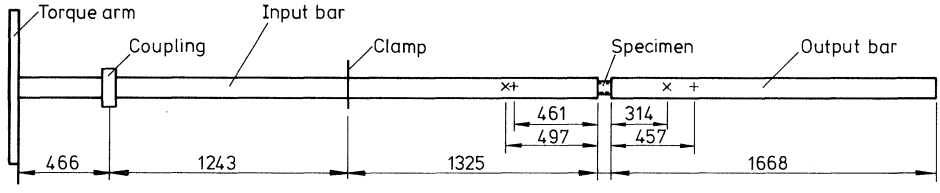

Figure 14. Split Hopkinson torsion bar. All dimensions are in millimetres.

A clamp is placed at the mid-point of the input bar and the free top end of this bar is given a prescribed torque Q using dead loading. On release of the clamp a torsional wave of magnitude $\frac{1}{2}Q$ travels along the input bar from the clamp to the specimen at the elastic shear wave speed of titanium ($c = 3100$ m s^{-1}). A portion of torque Q_T is transmitted through the specimen into the output bar, while the remainder $\frac{1}{2}Q - Q_T$ is reflected back into the input bar. Strain gauges are placed on the two bars to record the torque histories. The strain signals are amplified and recorded on a digital storage oscilloscope.

Theory

By simple one dimensional wave theory, the torsional impedance of both input and output bars is $J\rho c$, where c is the shear wave speed, ρ is the density of bar material and J is the polar moment of area of the bar. The angular velocity ω_T of the ouput bar is given by:

$$\omega_T = Q_T/J\rho c, \tag{A 1}$$

where torque Q_T is deduced at any instant from the strain gauge measurement on the output bar. The angular velocity ω_I of the upper face of the specimen connected to the input bar is:

$$\omega_I = (\tfrac{1}{2}Q - Q_T)/J\rho c, \tag{A 2}$$

where $\frac{1}{2}Q - Q_T$ is deduced from the strain gauge measurement on the input bar.

The specimen is short enough for the time of passage of a stress wave through it to be negligible, thus the twist of the specimen $\Delta\omega$ is given by:

$$\Delta\omega = \omega_I - \omega_T = (Q - 2Q_T)/J\rho c. \tag{A 3}$$

The shear stress τ on the specimen at any instant is assumed to equal the average shear stress at the gauge section:

$$\tau = Q_T/2\pi r^2 t, \tag{A 4}$$

where r is the mean of the outer and inner radii of the tubular specimen and t is the wall thickness. The shear strain-rate $\dot{\gamma}$ of the gauge section is:

$$\dot{\gamma} = \Delta\omega r/l, \tag{A 5}$$

where l is the height of the gauge section. Integration of the strain-rate with respect to time gives the shear strain imposed on the specimen.

The above analysis assumes that the gauge length of the specimen is sufficiently short for the specimen to suffer a uniform strain rate. This assumption is reasonable since the time required for an elastic stress wave to traverse the gauge length of the specimen is typically 1 μs, compared with a test time of 1 ms.

In several of the tests the transmitted torque Q_T is negligible compared with the incident torque $\frac{1}{2}Q$. Then ω_I, $\Delta\omega$, and $\dot{\gamma}$ are almost constant during a test by equations (A 2), (A 3) and (A 5) respectively. Under these conditions, the strain-time response from the gauge on the output bar is of the same shape as the $\tau-\gamma$ response of the specimen. In presenting results however, both the Q_T and Q histories were used in the calculation of the $\tau-\gamma$ curves.

Design chart

A design chart may be constructed showing the successful range of strain rates $\dot{\gamma}$ and torques Q which the Hopkinson bar can apply to the polymer specimens.

The strain rate $\dot{\gamma}$ imposed on the specimen depends upon the specimen geometry, the shear yield stress of the specimen and the torque Q on the input torsion bar. The achievable strain rate for a specimen made from rigid perfectly plastic material of shear yield stress 60 MPa, mean radius 9 mm and wall thickness 0.5 mm is plotted as a function of torque Q in figure 15. When Q is too small the

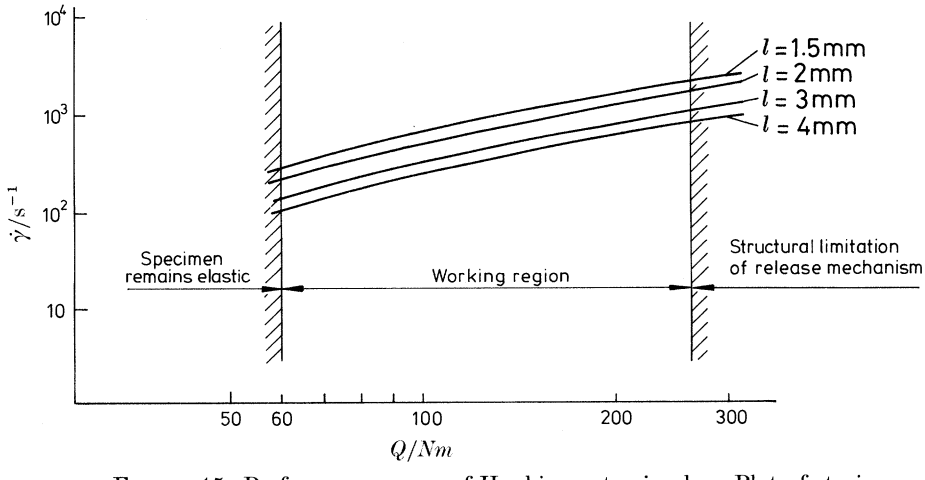

FIGURE 15. Performance range of Hopkinson torsion bar. Plot of strain rate $\dot{\gamma}$ achievable from an input torque Q.

specimen does not yield; when Q is too large the clamp is unable to secure the input bar. Thus an operating régime is defined in $\dot{\gamma}$–Q space. In the present tests, a gauge length $l = 4$ mm is used for $\dot{\gamma} < 800\ \mathrm{s}^{-1}$ and a gauge length $l = 1.5$ mm is used for higher strain rates $\dot{\gamma} > 800\ \mathrm{s}^{-1}$.

The maximum strain γ which the split torsion bar can impose on the specimen is fixed by the time of travel of a shear wave from the clamp to the top of the input bar and thence to the specimen at the other end of the input bar. Typically, for a strain rate of $\dot{\gamma} = 500\ \mathrm{s}^{-1}$ the maximum measurable strain is $\gamma = 0.45$; for a strain rate $\dot{\gamma} = 2000\ \mathrm{s}^{-1}$, the maximum measurable strain is $\gamma = 1.8$.

Environmental chamber

For tests at above ambient temperature the specimen is heated *in situ* in a tubular electrical resistance furnace. Tests at temperatures below ambient are performed by surrounding the specimen with a perforated copper coil. Cooled nitrogen gas is sprayed onto the specimen from the coil, using the arrangement described in Clyens *et al.* (1982). Test temperature is monitored using a chromel–alumel thermocouple placed in contact with the specimen. The high rate test is performed when the temperature of the specimen attains the required value.

References

Argon, A. S. 1973 *Phil. Mag.* **28**, 839–865.

Argon, A. S. & Hannoosh, J. G. 1977 *Phil. Mag.* **36**, 1195.

Bai, Y. L. 1982 *J. Mech. Phys. Solids* **30** (4), 195–207.

Bauwens, J. C. 1972 *J. mater. Sci.* **7**, 577–584.

Bauwens-Crowet, C. 1973 *J. mater. Sci.* **8**, 968–979.

Bauwens-Crowet, C., Bauwens, J. C. & Homes, G. 1972 *J. mater. Sci.* **7**, 176–183.

Billington, E. W. & Brissenden, C. 1971 *Int. J. mech. Sci.* **13**, 531.

Briscoe, B. J. & Nosker, R. W. 1984 *Wear* **95**, 241.

Brown, N. 1971 *Bull. Am. phys. Soc.* **16**, 428.

Clyens, S., Evans, C. R. & Johnson, K. L. 1982 *Proc. R. Soc. Lond.* A **381**, 195–214.

Cottrell, A. H. 1963 *The mechanical properties of matter*, p. 284. Wiley.

Donald, A. M. & Kramer, E. J. 1982 *J. Polym. Sci., Polym. Phys. Edn* **20**, 899.

Donald, A. M., Kramer, E. J. & Bubeck, R. A. 1982 *J. Polym. Sci., Polym. Phys. Edn* **20**, 1129.

Fleck, N. A. 1990 Brittle fracture due to an array of microcracks. *Proc. R. Soc. Lond.* A. (Submitted.)

Fuller, K. N. G., Fox, P. G. & Field, J. E. 1975 *Proc. R. Soc. Lond.* A **382**, 231–244.

G'Sell, C. 1985 *Proc. 7th Int. Conf. Strength of Metals and Alloys, Montreal, Canada, 12–16 August 1985* (ed. H. J. McQueen, J. P. Bailon, J. I. Dickson, J. J. Jonas & M. G. Akben), vol. 3, pp. 1943–1983.

G'Sell, C. & Gopez, A. J. 1985 *J. mater. Sci.* **20**, 3462–3478.

Haward, R. N. & Thackray, G. 1968 *Proc. R. Soc. Lond.* A **302**, 453.

Hull, D. 1975 *Polymeric materials*, ch. 9, pp. 487–550. Metals Park, Ohio: ASM.

Iwayanagy, S. & Hideshima, T. 1953 *J. phys. Soc. Japan* **8**, 368.

Kinloch, A. J. & Young, R. J. 1983 *Fracture behaviour of polymers*. Applied Science Publications.

Kolsky, H. 1949 *Proc. phys. Soc. Lond.* B **62**, 676.

Locati, G. & Tobolsky, A. V. 1970 *Adv. mol. Relaxation Processes* **1**, 375.

McClintock, F. A. & Stowers, I. F. 1970 Research memorandum no. 159, Fatigue and Plasticity Laboratory, Mechanical Engineering Department, M.I.T., Cambridge, U.S.A.

Radin, J. & Goldsmith, W. 1988 *Int. J. Impact Engng* **7** (2), 229–259.

Ree, T. & Eyring, J. 1958 *Rheology* (ed. F. R. Eirich), vol. 2, ch. 3.

Robertson, R. E. 1963 *J. appl. Polym. Sci.* **7**, 443.
Sherby, O. D. & Dorn, J. E. 1958 *J. Mech. Phys. Solids* **6**, 145.
Steer, P. 1985 These de Docteur en Science des Materiaux, no. 16, Univ. des Sciences et Techniques de lille, Flanders Artois.
Thompson, E. V. 1968 *J. Polymer Sci.* A2, **6**, 433.
Walley, S. M., Field, J. E., Pope, P. H. & Safford, N. A. 1989 *Phil. Trans. R. Soc. Lond.* A **328**, 1–33.
Ward, I. M. 1983 *The mechanical properties of solid polymers*, 2nd edn. Wiley.
Winter, R. E. 1975 *Phil. Mag.* **31**, 765–773.
Zhurkov, S. N. 1965 *Int. J. Fract. Mech.* **1**, 311–323.